



Global Biogeochemical Cycles

RESEARCH ARTICLE

10.1002/2016GB005424

Key Points:

- Increased biogenic silica fluxes with depth imply nonsteady state conditions in the NE Atlantic in August 2009
- Taxonomic flux analysis and simple modeling support the nonsteady state hypothesis
- By assuming steady state, net organic carbon supply to the dark ocean may be wrong by $\leq 25\%$

Correspondence to:

S. L. C. Giering,
s.giering@noc.ac.uk

Citation:

Giering, S. L. C., R. Sanders, A. P. Martin, S. A. Henson, J. S. Riley, C. M. Marsay, and D. G. Johns (2017), Particle flux in the oceans: Challenging the steady state assumption, *Global Biogeochem. Cycles*, 31, 159–171, doi:10.1002/2016GB005424.

Received 8 APR 2016

Accepted 30 DEC 2016

Accepted article online 2 JAN 2017

Published online 28 JAN 2017

Particle flux in the oceans: Challenging the steady state assumption

Sarah L. C. Giering¹ , Richard Sanders¹ , Adrian P. Martin¹ , Stephanie A. Henson¹ , Jennifer S. Riley¹, Chris M. Marsay^{2,3} , and David G. Johns⁴ 

¹National Oceanography Centre, European Way, Southampton, UK, ²Ocean and Earth Science, University of Southampton, Southampton, UK, ³Now at Skidaway Institute of Oceanography, University of Georgia, Savannah, Georgia, USA, ⁴Sir Alister Hardy Foundation for Ocean Science, The Laboratory, Citadel Hill, Plymouth, UK

Abstract Atmospheric carbon dioxide levels are strongly controlled by the depth at which the organic matter that sinks out of the surface ocean is remineralized. This depth is generally estimated from particle flux profiles measured using sediment traps. Inherent in this analysis is a steady state assumption that export from the surface does not significantly change in the time it takes material to reach the deepest trap. However, recent observations suggest that a significant fraction of material in the mesopelagic zone sinks slowly enough to bring this into doubt. We use data from a study in the North Atlantic during July/August 2009 to challenge the steady state assumption. An increase in biogenic silica flux with depth was observed which we interpret, based on vertical profiles of diatom taxonomy, as representing the remnants of the spring diatom bloom sinking slowly ($<40 \text{ m d}^{-1}$). We were able to reproduce this behavior using a simple model using satellite-derived export rates and literature-derived remineralization rates. We further provide a simple equation to estimate “additional” (or “excess”) particulate organic carbon supply to the dark ocean during nonsteady state conditions, which is not captured by traditional sediment trap deployments. In seasonal systems, mesopelagic net organic carbon supply could be wrong by as much as 25% when assuming steady state. We conclude that the steady state assumption leads to misinterpretation of particle flux profiles when input fluxes from the upper ocean vary on the order of weeks, such as in temperate and polar regions with strong seasonal cycles in export.

1. Introduction

The depth at which carbon exported from the surface ocean is recycled is a key control over ocean atmosphere carbon dioxide partitioning [Kwon *et al.*, 2009]. Some of the earliest systematic observations of particle flux were made by Martin *et al.* [1987] who deployed sediment traps off the west coast of the U.S. in the mesopelagic zone (100–1000 m) and found that particle flux decreased with depth and was best described by a power law function, now commonly known as the Martin curve. Even though this function was chosen purely as the best fit, with no underlying theoretical justification, it is now widely used to model flux attenuation in ocean models (e.g., in all of the models used in the Ocean-Carbon Cycle Model Intercomparison Project) [Sarmiento and LeQuere, 1996; Doney *et al.*, 2004] and to extrapolate measured fluxes to different depths.

Flux profiles acquired using sediment traps or estimated using the Martin curve are commonly assumed to be at steady state, partly because of reported rapid sinking speeds of aggregates: up to 400 m d^{-1} for marine snow and 1800 m d^{-1} for fecal pellets (see review by Turner [2002]). Imagine a scenario of two traps collecting material at 50 m and 850 m depth. At an average sinking speed of 400 m d^{-1} , material collected at 850 m would have been at 50 m around 2 days before. Unless there was a significant change in export at 50 m over 2 days then the steady state assumption is valid. Accurate simultaneous flux measurements are necessary to understand the ocean carbon cycle, for example, when comparing the observed loss of sinking particulate carbon in the mesopelagic zone with estimates of heterotrophic respiration [Giering *et al.*, 2014].

However, recent observations [e.g., Alonso-González *et al.*, 2010; Villa-Alfageme *et al.*, 2014; Giering *et al.*, 2016], including some from the cruise reported here [Riley *et al.*, 2012], suggest that a significant fraction of the particle flux in the oceans may sink at much slower speeds ($<40 \text{ m d}^{-1}$). If this is the case, particles may take several weeks to sink from the surface ocean to the deep ocean. For the steady state assumption to be valid, the timescale over which the flux leaving the surface ocean needs to be constant must therefore be considerably longer, extending from a few days to several months. Yet a large proportion of the ocean

exhibits seasonal variability in primary production and phytoplankton standing stocks and may therefore also display variability in export flux. We hypothesize that in such systems the steady state assumption may not be valid.

We first undertake some theoretical modeling of how nonsteady state situations coupled with slowly sinking particles may affect vertical particle flux profiles. We then discuss data from a field site which shows the predicted pattern. Finally, we derive a simple equation to estimate the “additional” (or “excess”) POC supply to the dark ocean during nonsteady state conditions, which is not captured by traditional analyses of sediment trap deployments.

2. Methods

2.1. Nonsteady State Model

Some simple calculations help to examine how the presence of remnant particles at depth, owing to slow sinking speeds, affects particle flux profiles. The calculations are based on the assumption that the sinking speed and particle remineralization rates are constant with depth and during the time period considered. Commonly, particle flux is described by assuming a power law function [Martin *et al.*, 1987]. This function relates the flux at a target depth z (F_z) to the flux at a shallower reference depth z_0 using the equation $F_z = F_{z_0}(z/z_0)^{-b}$, where b describes the rate of flux attenuation. In this case, there is an implicit assumption that either sinking speed increases with depth or remineralization rate decreases as the particle sinks [e.g., Gehlen *et al.*, 2006; Villa-Alfageme *et al.*, 2014]. Hence, to use the Martin curve would be inconsistent with our assumptions. An assumption of constant remineralization rate and sinking speed gives an exponential relationship rather than a power law one, and therefore, this was used when describing flux with depth. For the exponential model the rate of flux attenuation with depth is set by the choice of the two constants representing sinking speed and remineralization rate.

It is, however, important to note that particles in the oceans do not have a universal sinking speed or remineralization rate [e.g., Alonso-González *et al.*, 2010; McDonnell and Buesseler, 2010]. Rather, particles experience diversity in both rates, which could in itself cause the shape of idealized flux curves or departures therefrom [e.g., Boyd and Trull, 2007]. Along these lines, a previous study measured the distribution of sinking rates and demonstrated that the variability in these could have produced an apparent Martin curve without any changes in sinking rates or remineralization rates because slow-sinking particles are lost at a shallower depths and only fast-sinking particles reach deeper waters [Trull *et al.*, 2008]. Such selective losses would also explain the overall faster bulk sinking rates observed with increasing depth [Berelson, 2002; Villa-Alfageme *et al.*, 2014, 2016]. It is, however, widely accepted that the processes that shape particle flux profiles are more complex and involve, amongst others, physical or zooplankton-mediated fragmentation and aggregation [e.g., Conte *et al.*, 2001; Trull *et al.*, 2008; Burd and Jackson, 2009; Giering *et al.*, 2014]. In order to explore the effect of nonsteady state conditions, we refrain from adding these complexities and focus on a simple particle flux scenario by assuming a fixed sinking speed and remineralization rate.

We simulated a series of downward flux profiles at 8 day intervals over a 60 day period. The input of matter from the mixed layer (“export flux,” F_{in}) was chosen to decrease over time at a rate (α) of $1.2 \text{ mg m}^{-2} \text{ d}^{-1}$, simulating declining phytoplankton standing stocks during the postbloom phase (-1 to $-1.6\% \text{ d}^{-1}$) [Henson *et al.*, 2013, Figure 1b]. Export flux on our simulated observation date (at the end of the 60 day period) was $28 \text{ mg m}^{-2} \text{ d}^{-1}$ ($F_{in,0} = 28 \text{ mg m}^{-2} \text{ d}^{-1}$). F_{in} at a time Δt earlier than the simulated profile can thus be calculated as

$$F_{in,\Delta t} = F_{in,0} + \alpha \Delta t \quad (1)$$

Flux attenuation with depth was calculated by applying an exponential decay model with both a weak remineralization rate ($r = 0.01 \text{ d}^{-1}$) and a strong remineralization rate ($r = 0.20 \text{ d}^{-1}$). The flux observed at depth $z_{\Delta t}$ will have left the surface at a time $\Delta t = z_{\Delta t}/v$ days earlier, where v is the particle sinking speed (m d^{-1}). The relation between the flux leaving the surface and that observed at depth z is therefore

$$F(z_{\Delta t}) = F_{in,\Delta t} \exp(-rz_{\Delta t}/v) = F_{in,\Delta t} \exp(-r\Delta t) \quad (2)$$

where $F_{in,\Delta t}$ is the export flux Δt days before the observation (see equation (1)) and r is the flux attenuation coefficient (day^{-1}). For our simulation, we assume that particles sink at a speed of 10 m d^{-1} [Alonso-González *et al.*, 2010; Riley *et al.*, 2012]. For a particle profile collected on 1 day, a trap deployed at 200 m below the

mixed layer would capture particles that were exported from the surface 20 days ago, while a trap at 600 m below the mixed layer would collect 60 day old particles. This “observed” profile is hereafter referred to as “composite profile.”

2.2. Potential Error When Estimating Net POC Supply

We can further use equations (1) and (2) to calculate both the apparent loss of POC from a composite profile—as traditionally observed during deployments of a fleet of five sediment traps—and the actual loss of POC. “Loss” is here synonymous with the net POC supply between the top and bottom trap depths. We assume again that remineralization rate and sinking speed do not change over time.

To calculate the apparent loss between two depths a vertical distance $\Delta z = v \times 1$ day apart, we simply subtract the observed flux at the deeper depth from the observed flux at the shallower depth (e.g., $F_{50m} - F_{100m}$). Let us consider the two depths corresponding to those which material would sink to in Δt and $\Delta t - 1$ days. The apparent loss (L_{app}) is hence calculated using equation (1) as

$$L_{app} = F_{in,\Delta t-1} \exp(-z_{\Delta t-1}r/v) - F_{in,\Delta t} \exp(-z_{\Delta t}r/v) \quad (3)$$

The actual loss (L_{act}), on the other hand, is the difference between the observed flux at one reference depth and the flux at a shallower depth that originated from the same input flux, $F_{\Delta t}$:

$$L_{act} = F_{in,\Delta t} [\exp(-z_{\Delta t-1}r/v) - \exp(-z_{\Delta t}r/v)] \quad (4)$$

We can calculate the difference between the actual loss and the apparent loss at depth z ($D_z = L_{act} - L_{app}$) by combining equations (3) and (4), substituting with equation (1), and simplifying to

$$D_z = \alpha \exp(-z_{\Delta t-1}r/v) \quad (5)$$

Using the sum for finite geometric series, the sum throughout the water column is

$$S = \alpha [1 - \exp(-r \times t_{max})] / [1 - \exp(-r)] \quad (6)$$

where t_{max} is the length of time corresponding to the depth (relative to the mixed layer depth or photic zone depth) of the deepest sample divided by the assumed sinking speed ($t_{max} = z_{max}/v$). This sum, S , allows quantification of how much the net organic carbon supply to the mesopelagic zone may be underestimated or overestimated when assuming steady state. This calculation can easily be applied wherever there is information about α , r , and v .

2.2.1. Case Study: Porcupine Abyssal Plain (PAP) Site

The theoretical model described above was applied to the PAP data (see section 2.3) and a sensitivity analysis was performed. The parameters were chosen to reflect likely conditions at the PAP site. During the 60 days prior to our cruise, POC export decreased according to satellite-derived data at a rate of $1.1 \text{ mg C m}^{-2} \text{ d}^{-1}$ (linear regression; $p < 0.01$, $R^2 = 0.73$, $n = 8$). POC has been shown to be remineralized at $0.08\text{--}0.20 \text{ day}^{-1}$ [Iversen and Ploug, 2010], and average sinking speeds at the PAP site were likely between 20 and 100 m d^{-1} [Riley et al., 2012; Villa-Alfageme et al., 2014]. To represent uncertainties, we thus varied the parameters for temporal decrease in organic matter export from the mixed layer (α ; $0.5\text{--}1.3 \text{ mg C m}^{-2} \text{ d}^{-1}$), remineralization rate (r ; $0.01\text{--}0.50 \text{ day}^{-1}$), and sinking speed (v ; $10\text{--}200 \text{ m d}^{-1}$).

2.2.2. Seasonal Examples Using Atlantic and Pacific Transects

To illustrate how the potential range of error when assuming steady state may vary geographically and seasonally, we applied equation (6) to satellite-derived export estimates (see section 2.4). We use climatological mean (2003–2014) estimates with temporal resolution of 8 days and spatial resolution of 1° . The change in export flux from the upper 100 m (α) was calculated at every grid cell for each time step as the gradient over an 8 day period. S was then calculated using a sinking speed v of 40 m d^{-1} , z_{max} of 400 m (i.e., 500 m depth), and a remineralization rate scaled with a temperature coefficient (Q_{10}) of 3.5 [Iversen and Ploug, 2013]:

$$r = 0.03 \text{ d}^{-1} \times Q_{10}^{\frac{T-4^\circ\text{C}}{10^\circ\text{C}}} \quad (7)$$

where 0.03 d^{-1} and 4°C are the reference rates [Iversen and Ploug, 2013], and T is the satellite-derived sea surface temperature (SST) in $^\circ\text{C}$. We chose a Q_{10} of 3.5 as this value is based on measurements of carbon-specific respiration on diatom aggregates [Iversen and Ploug, 2013] and is similar to the Q_{10} measured for growth rates of pelagic bacteria ($Q_{10} = 3.3$) [White et al., 1991]. To test the effect of this choice, we also recalculated our analysis using a Q_{10} of 2. The patterns are the same for the two Q_{10} values, but a Q_{10} of 2 suggests a more

Table 1. Potential Underestimation of Organic Matter Supply to the Dark Ocean, Integrated Between 0 and 950 m Below the Mixed Layer (50 m Deep), as a Function of Remineralization Rate (r ; day^{-1}), Sinking Speed (v in m d^{-1}), and Associated Δt in Days), and Decrease in Export Flux Over Time (a ; Here in $\text{mg C m}^{-2} \text{d}^{-1}$)^a

		$a = 1.1 \text{ mg C m}^{-2} \text{d}^{-1}$						$v = 50 \text{ m d}^{-1}$						
v	Δt	r						a						
		-0.01	-0.02	-0.05	-0.1	-0.2	-0.5	-0.01	-0.02	-0.05	-0.1	-0.2	-0.5	
10	95	68	47	22	12	6	3	0.5	9	8	6	4	3	1
20	48	42	34	20	11	6	3	0.7	12	11	9	6	4	2
50	19	19	18	14	10	6	3	0.9	16	14	11	8	5	2
100	10	10	10	9	7	5	3	1.1	19	18	14	10	6	3
200	5	5	5	5	4	4	3	1.3	23	21	16	12	7	3

^aLight and dark grey shaded areas show, respectively, likely and most likely combinations at the PAP site during August 2009.

extreme over/underestimate of global export. This is because a lower Q_{10} suggests lower remineralization rates when $SST > 4^\circ\text{C}$, which leads to a stronger nonsteady state effect in these regions (see Table 1 and Figure 7). To test the sensitivity of S , we calculated S at four “example” sites in both the Atlantic and Pacific (50°N , 35°W ; 40°S , 35°W ; 50°N , 175°W ; and 40°S , 175°W) using a range of sinking speeds (10, 40, and 200 m d^{-1}) and remineralization rates (0.01, 0.03, and 0.09 d^{-1}). As we are interested in illustrating the relative uncertainty in sinking flux due to nonsteady state effects, S was normalized to the daily export flux.

To test the sensitivity of our results to the choice of satellite-derived primary production (PP) and e -ratio algorithm (see section 2.4), we also calculated S normalized to daily export flux at the four example sites using 12 permutations of commonly used algorithms. We used PP algorithms of Carr [2001] and Marra et al. [2003] and the Vertically Generalized Production Model (VGPM [Behrenfeld and Falkowski, 1997]). Export production was estimated using the empirical algorithms by Dunne et al. [2005], Henson et al. [2011], and Laws et al. [2000], in addition to the food web model of Laws et al. [2000]. The procedure followed is the same as in the supplementary information of Henson et al. [2012].

2.3. Case Study Sampling Site and Particle Collection

Samples were collected at the PAP site (49.0°N , 16.5°W) from 8 July to 13 August 2009 aboard the RRS *Discovery* (D341 Cruise report [Sanders, 2009]). The mixed layer depth was $\sim 50 \text{ m}$ throughout the study period [Giering et al., 2014], and this depth is used as the reference depth for export throughout this study. Sinking flux was measured using free-drifting, neutrally buoyant sediment traps (PELAGRA [Lampitt et al., 2008]). PELAGRA traps were deployed at depths between 50 and 670 m over a period of 4 weeks (Figure 1). A total of 16 successful PELAGRA deployments were conducted to acquire four depth profiles of particle flux.

Sample cups for each trap contained filtered seawater (5 ppt excess salinity) and chloroform (at saturating concentrations). Sample cups were closed during the first 18–24 h of each deployment until traps reached, and stabilized at, the programmed depth.

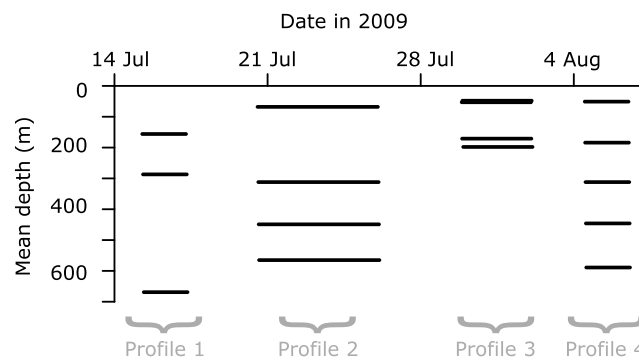


Figure 1. Details for the four PELAGRA profiles. Deployment period and mean depth for each PELAGRA deployment is indicated by a horizontal line, which marks the opening and closing of the sample cups.

Then, cups opened to collect sinking material for 48–132 h, before closing again for the ascent and trap recovery. For each trap, the contents of two or three of the four sample cups were screened ($350 \mu\text{m}$ mesh) to remove swimmers and split into eight aliquots for analyses of biogenic silica (bSiO_2), community composition and other constituents of the vertical flux.

For bSiO_2 , aliquots were filtered through $0.8 \mu\text{m}$ pore polycarbonate membranes (Nuclepore, 25 mm diameter) while at sea and stored at

–20°C. Filters were dried (60°C, 24 h), then processed and analyzed using a method adapted from *Ragueneau and Treguer* [1994]. Filters were heated with 0.2 M sodium hydroxide for 90 min to dissolve bSiO₂ then cooled and neutralized with 0.1 M hydrochloric acid. The resulting solution was separated from remaining particulate material by centrifugation, and dissolved silicate was measured on a SEAL QuAATro autoanalyzer. Results were converted to mass of bSiO₂ by assuming a molecular mass of 60. No replicate analyses for bSiO₂ were carried out during this work, but previous replicate measurements by PELAGRA traps [Salter *et al.*, 2007; Martin *et al.*, 2011] suggest a relative standard deviation of 10% between replicate aliquots.

For community composition, aliquots were preserved in 2% borax-buffered formaldehyde and stored in a cool, dark place until further analysis. One mL of the preserved flux material was diluted with alkaline deionized water (pH 9) to make up 10 mL. The solution was split in half and filtered onto cellulose nitrate filters (0.8 μm nominal pore size, 25 mm diameter), rinsed with alkaline deionized water (pH 9), and dried (30°C, 8 h). Half of each filter was mounted on a glass slide with cover slit using Norland Optical Adhesive (Technoptics) and cured in UV light. Diatoms were counted under plain light at 400X magnifications using a polarizing light microscope (Brunel SP200) and identified to species level.

In addition, 30 marine snow aggregates were collected from the base of the mixed layer (~50 m) using the Marine Snow Catcher (MSC) [Riley *et al.*, 2012] and analyzed for diatom composition following the method above. The taxonomic composition of diatoms in the mixed layer was determined from 100 mL water samples collected at 5, 25, and 50 m depth using Niskin bottles. Samples were preserved with 2 mL Lugol's iodine solution and stored in a dark, cool place. On shore, cells were allowed to settle for 12 h, and diatoms were counted and identified using an inverted microscope (Brunel SP951).

2.4. Satellite-Derived Fluxes at the PAP Site

Fluxes of bSiO₂ at 50 m (export flux) were estimated from satellite-derived POC flux data. We estimated downward POC flux from the surface ocean using satellite data following *Henson et al.* [2011]. An empirical relationship between the export ratio (export/primary production) and SST was derived from a database of 306 observations of particle export: $e\text{-ratio} = 0.23 \times \exp(-0.08 \times \text{SST})$. We applied this equation to satellite-derived SST (MODIS Aqua) at 8 day resolution for a 1° region around the PAP site. The e -ratio estimates were then multiplied by satellite-derived PP calculated using the algorithm by *Carr* [2001], again at 8 day temporal resolution, giving an estimate of export in $\text{mg C m}^{-2} \text{d}^{-1}$.

POC fluxes were converted to bSiO₂ fluxes using a bSiO₂:POC ratio that varies with the time of year. We extracted this information for the region of the PAP site (47–49°N, 16–21°W) from data sets of sediment trap observations during the North Atlantic Bloom experiment [Honjo and Manganini, 1992; Lampitt *et al.*, 2001; Torres Valdés *et al.*, 2014]. The traps ($n = 26$) were deployed between 1000 and 1200 m depth between the years 1989–1990. The data reveal a seasonal pattern in bSiO₂:POC (Figure 2a), which we fitted with a cyclic spline smoother ($R^2 = 0.76$, $n = 26$). The bSiO₂:POC ratios at ~1000 m depth are likely to be higher than the corresponding surface ratios due to preferential recycling of POC [Martin *et al.*, 2011]. During our cruise, for example, average bSiO₂:POC ratios of slow-sinking particles and total flux at 50 m were, respectively, $0.065 \pm 0.031 \text{ mg mg}^{-1}$ [Riley *et al.*, 2012] and $0.021 \pm 0.013 \text{ mg mg}^{-1}$ (this study, using POC measurements from the same trap samples), whereas the deep sediment trap record shows a bSiO₂:POC ratio of ~1.4 mg mg^{-1} (Figure 2a). We therefore scaled the time series accordingly (bSiO₂:POC at surface = scaling_factor × bSiO₂:POC at 1000 m) using an average scaling factor (bSiO₂:POC_{surface}/bSiO₂:POC_{1000m}) of 0.03 and bracketed this value using lower and higher scaling factors of, respectively, 0.015 and 0.046. We acknowledge that the uncertainties of this ratio are large and that the ratio of bSiO₂:POC_{surface}/bSiO₂:POC_{1000m} likely varies throughout the year; however, we consider it sufficient for the purpose of this study, which is to discuss general assumptions rather than to calculate absolute rates.

3. Results and Discussion

3.1. Increase of Fluxes With Depth

The results of the two nonsteady state simulations (using $r = 0.01 \text{ day}^{-1}$ or $r = 0.20 \text{ day}^{-1}$) show that a combination of slow sinking speeds and weak remineralization during a period of declining surface export can lead to an apparent increase of particle flux with depth (Figures 3a–3c). On the other hand, a combination of slow sinking speeds, strong remineralization, and declining surface export results in profiles following

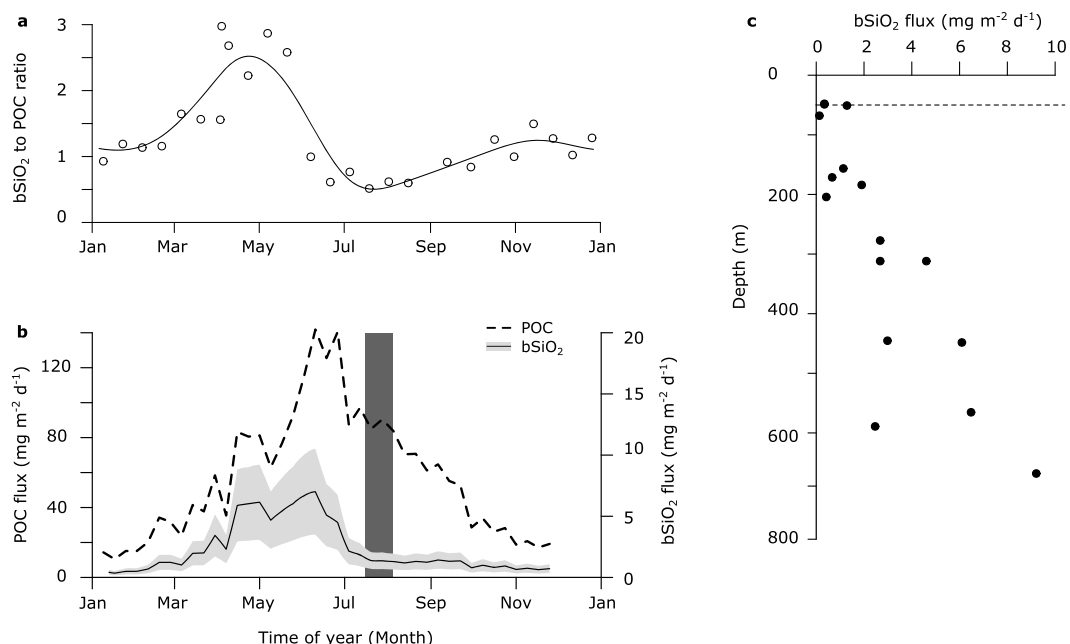


Figure 2. (a) Ratio of bSiO₂ to POC at the PAP site. Flux was collected using sediment traps at 1000–1200 m depth during 1989–1990 at the PAP site [Honjo and Manganini, 1992, Lampitt *et al.*, 2001; Torres-Valdes *et al.*, 2014] and bSiO₂:POC ratio calculated ($\text{mg SiO}_2 \text{ mg}^{-1} \text{ POC}$). Line shows fit with cyclic spline smoother ($p < 0.001$, $R^2 = 0.76$, $n = 26$). (b) Satellite time series of particulate organic carbon (POC) export (dashed line) and bSiO₂ export (solid line). Shaded area (light grey) shows uncertainty of bSiO₂ export. The time of the cruise is highlighted in dark grey. (c) Depth profile of bSiO₂ fluxes as measured using PELAGRA during our study. Dashed line: average mixed layer depth during the study.

the expected decrease with depth (Figures 3a, 3d, and 3e) because the greater remineralization rate compensates for the effects of slow sinking speeds and decreasing export.

We now present data from the PAP site in the North Atlantic, where we observed an increase of bSiO₂ fluxes with depth. A thorough analysis of the site suggests that this apparent increase could have indeed been caused by nonsteady state conditions.

3.2. Case Study: PAP Site

The sediment trap deployments showed that bSiO₂ fluxes increased systematically with depth (Figure 2c). Fluxes ranged between 0.13 and 1.3 $\text{mg bSiO}_2 \text{ m}^{-2} \text{ d}^{-1}$ at 50 m and increase to 2.5–9.2 $\text{mg bSiO}_2 \text{ m}^{-2} \text{ d}^{-1}$ below 500 m. The observed increase of bSiO₂ fluxes with depth is surprising as bSiO₂ is undersaturated in the oceans, with an estimated 55–60% of sinking bSiO₂ dissolving in the upper 100 m on a global scale [Nelson *et al.*, 1995]. The increase with depth has four possible explanations: (a) there is a significant internal source of bSiO₂, (b) there is a lateral advection of material, (c) sediment traps near the surface fail to collect the entirety of the flux, or (d) the steady state assumption is incorrect.

bSiO₂ (commonly referred to “opal”) is produced from silicate by specific organisms, including diatoms, radiolarian, silicoflagellates, and siliceous sponges as part of their skeletal structures. Though the production of bSiO₂ is not dependent on light availability, most occurs in the surface ocean with diatoms being the dominant producer [Nelson *et al.*, 1995; Ragueneau *et al.*, 2000]. We therefore assume that the observed increase of bSiO₂ flux at depth is not driven by internal sources of bSiO₂.

Another potential source of bSiO₂ at depth is laterally advected material. Alonso-González *et al.* [2009] found that lateral transport of POC from the shelf in the subtropical Northeast Atlantic can reach further than 1000 km offshore and was up to 3 orders of magnitude larger than vertical fluxes. For the PAP site, however, flow field analysis (based on satellite-derived near-surface velocities) showed that no water mass reaching the site during our study period passed over the continental shelf during the 3 months preceding the study [Giering *et al.*, 2014].

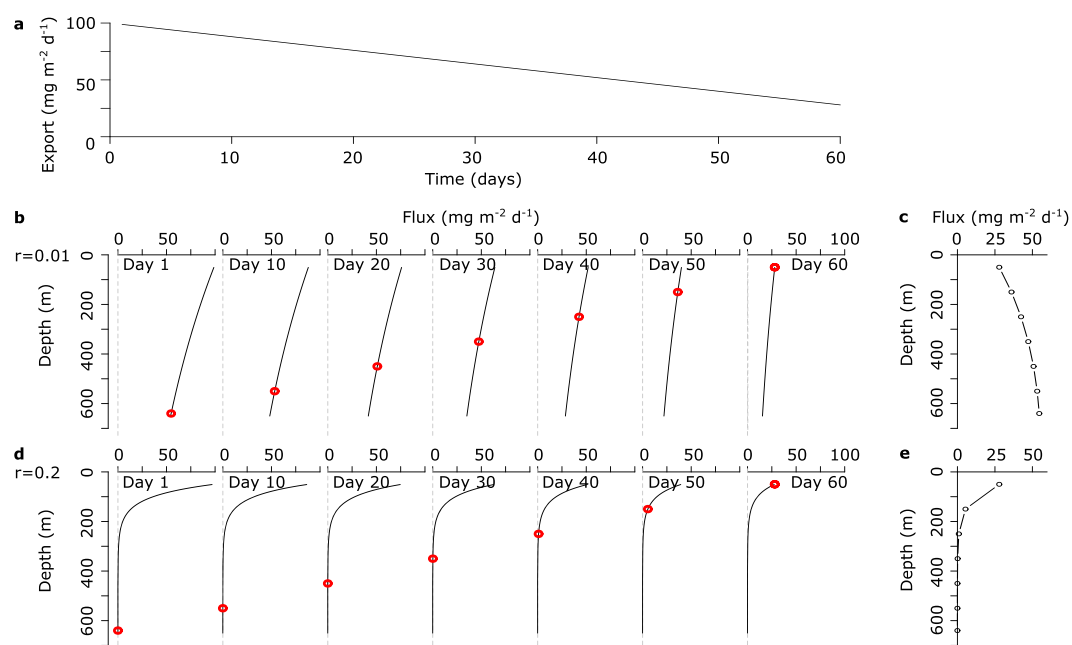


Figure 3. Simulation of how the presence of remnant particles at depth affects particle flux profiles. (a) Export flux at 50 m for the simulation period. Depth profiles of particle flux between days 1 and 60 when assuming remineralization rate r of (b) 0.01 and (d) 0.20. Red circles show the flux sampled by a hypothetical sediment trap deployed at day 60 if particles sank at 10 m d^{-1} . Depth profiles of particle flux as seen by hypothetical sediment traps deployed at day 60 if particles sank at 10 m d^{-1} and (c) $r = 0.01 \text{ day}^{-1}$ or (e) $r = 0.20 \text{ day}^{-1}$.

Even when using Lagrangian sediment traps, such as PELAGRA, source and collection sites can vary. At the study site ALOHA (A Long-term Oligotrophic Habitat Assessment) in the subtropical Pacific Ocean, for example, the source of the particles captured in the traps at 500 m depth was likely up to 25 km from the trap location [Siegel *et al.*, 2008]. Although we do not have in situ current data, an analysis of modeled surface currents (from $\frac{1}{4}^\circ$, 5 day NEMO) suggests that the source region of particles captured by the sediment traps was at most 100 km distant. Satellite Chl data from this region and during the deployment period suggest relatively homogeneous surface conditions, with Chl ranging from 0.45 to 0.75 mg Chl m⁻³ along the tracks. Moreover, during our study the PELAGRAS collected particles from an area covering $\sim 9100 \text{ km}^2$ over a period of 25 days; yet the increase in bSiO₂ flux with depth was apparent across all profiles (Figure 2c). We therefore conclude that lateral advection of bSiO₂ was likely negligible during our study.

We have also considered the possibility that the collection efficiency of PELAGRA increases with depth [Buesseler *et al.*, 2007]. Low collection efficiency at shallow depths coupled to a slow decline in flux with depth could lead to an apparent increase of flux with depth. During our study cruise, we conducted an extensive comparison of PELAGRA-derived fluxes out of the mixed layer ($\sim 50 \text{ m}$) with those obtained from the ²³⁴Th technique, MSC [Riley *et al.*, 2012], and satellites (Figure 2b). Estimated POC fluxes were 84 ± 2 , 99 ± 41 , 146 ± 26 , and $88 \pm 5 \text{ mg C m}^{-2} \text{ d}^{-1}$ according to PELAGRA, ²³⁴Th, MSC, and satellite-derived estimates, respectively. On the basis of this comparison, we do not believe that there was a systematic undertapping by PELAGRA in the surface.

It follows that a likely explanation for the observed increased bSiO₂ flux at depth is the invalidity of the steady state assumption. We hypothesize that the enhanced bSiO₂ flux at depth is the remnant of an earlier large flux of slowly sinking particles from the surface.

3.3. Challenging the Steady State Assumption

The simulation suggested that three conditions are needed in order to see an increase of flux with depth: (1) slow sinking speeds, (2) a period of declining surface export, and (3) low remineralization rates.

Slow sinking speeds. During our cruise, Villa-Alfageme *et al.* [2014] calculated bulk sinking speeds using ²¹⁰Po as a tracer and inverse modeling and estimated that particles sank, on average, at $88 (\pm 47 \text{ SD}) \text{ m d}^{-1}$ through the mesopelagic zone. This estimate agrees well with contemporaneous, indirect observations by Riley *et al.* [2012]

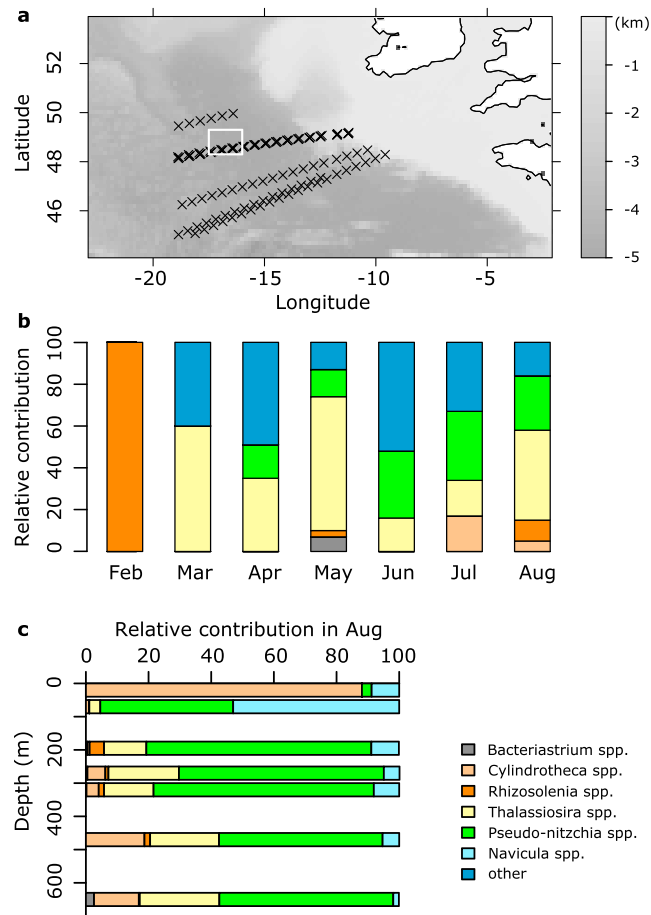


Figure 4. Changes in diatom population at the PAP site. (a) Sampling locations of the Continuous Plankton Recorder (CPR) survey in February–August 2009. White box shows PAP site area. (b) Relative contribution of different diatom species to total diatom abundance (based on cell counts in the CPR samples) in the upper ocean during February–August 2009. Colors represent species as in the key. (c) Changes of relative contribution with depth within the PAP site area in August 2009. Samples were collected using CPR (surface), Marine Snow Catcher (50 m), and PELAGRA sediment traps (175–630 m). Colors represent species as in the key.

which had only occurred in the upper ocean ~3 months prior to the cruise (Figure 4). Considering that *Bacteriastrum* spp. must have sunk out of the mixed layer ~40–70 days prior to the deployment of the deepest trap, this suggests that *Bacteriastrum* spp. sank at a speed of 8–15 m d⁻¹. The diatom *Cylindrotheca closterium* (cell length: 30–400 μm, cell width: 2–8 μm [Tomas, 1997]), on the other hand, only occurred in surface waters in July, yet were present in all traps during our cruise, including the deepest trap which had been deployed in mid-July (Figure 4). To reach this depth within 14 days, *Cylindrotheca* spp. would have to sink at ~40 m d⁻¹. It follows that the effective sinking speed of these diatoms was on the order of 8–40 m d⁻¹, which agrees with the observation that a significant fraction of particle flux is slow sinking [Alonso-González et al., 2010; Riley et al., 2012; Villa-Alfageme et al., 2014; Giering et al., 2016].

A period of declining surface export. Satellite-derived export estimates show that export flux was indeed declining in the weeks before our study. Throughout 2009, estimated export flux of POC and bSiO₂ at the PAP site ranged over one order of magnitude from ~20 mg POC m⁻² d⁻¹ and ~1 mg bSiO₂ m⁻² d⁻¹ in winter to 140 mg POC m⁻² d⁻¹ and 7 ± 3.5 mg bSiO₂ m⁻² d⁻¹ at the peak of the bloom (Figure 2b). For the 2 weeks immediately prior to the first sediment trap deployments (1 to 15 July) export was fairly constant, whereas during the preceding month (1 June to 1 July) export had declined rapidly (Figure 2b).

via the collection of fast- and slow-sinking particles at 50 m, which suggested that ~63% of the POC flux was sinking at <20 m d⁻¹ and 37% was sinking at 181 m d⁻¹ (resulting in a bulk sinking speed of ~73 ± 35 m d⁻¹). To support these indirect observations that slowly sinking particles can reach the lower mesopelagic zone, we ideally require a series of tracers that exit the surface ocean successively and thus indicate the age of particles at depth. The diatom population conveniently serves as such a tracer at the PAP site as it changes its taxonomic composition seasonally. Near-surface observations of the community structure are collected throughout the year as part of the Continuous Plankton Recorder (CPR) survey (www.sahfos.ac.uk). We compared the taxonomic composition of the CPR samples, determined via microscopy [Richardson et al., 2006], with the taxonomic composition of diatoms in our sediment traps, in the mixed layer and in marine snow aggregates collected at the bottom of the mixed layer.

The change in the species composition with depth in the trap samples was similar to the seasonal change in surface diatom composition. The deepest trap samples analyzed for species composition (630 m) contained diatoms of the genus *Bacteriastrum* (cell diameter: 5–56 μm [Tomas, 1997]),

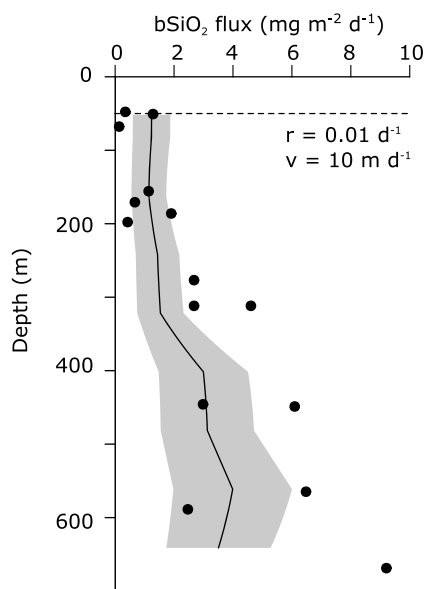


Figure 5. Comparison of observed bSiO_2 flux ($\text{mg bSiO}_2 \text{ m}^{-2} \text{ d}^{-1}$) at the PAP site during 6 Jun to 5 August 2009 (circles) and bSiO_2 flux profile calculated using satellite-derived estimates of bSiO_2 export and assuming sinking speeds of 10 m d^{-1} and remineralization rates of 0.01 day^{-1} (solid line). Grey area: uncertainty envelope expressing uncertainties in the scaling factor used for calculating bSiO_2 :POC ratios. Dashed line: average mixed layer depth during the study.

bSiO_2 at the PAP site was thus likely $\sim 1260 \mu\text{M}$ [Rickert *et al.*, 2002, equation 11], and k was likely between 9 and $15 \mu\text{mol g}^{-1} \text{ h}^{-1}$ [Rickert *et al.*, 2002, equation 10]. At silicate concentrations of $\sim 4 \mu\text{M}$ during our study (M. C. Stinchcombe, personal communication, 2016), the daily dissolution rate of bSiO_2 [Rickert *et al.*, 2002, equation 8] was thus probably in the order of $0.01\text{--}0.02 \text{ day}^{-1}$.

It appears that all of the three conditions that can lead to an apparent increase of flux with depth—slow sinking speeds, a period of declining surface export, and low remineralization rates—were present during our study. This strongly supports our hypothesis that parts of the deep flux are the remnants of export events that occurred several weeks previously.

Taking this a step further, we combine the derived rates of surface bSiO_2 export (Figure 2b), sinking speed (10 m d^{-1}) and a remineralization rate of 0.01 day^{-1} to produce depth profiles of particle flux as described for the nonsteady state model (equation (2)). The resulting flux profile matches the observed bSiO_2 flux reasonably well (Figure 5), supporting the hypothesis that the flux observed at depth could have been the remnants of the spring bloom. This calculation is, however, based on estimates with relatively large uncertainties and thus provides an illustrative example only.

We conclude that steady state conditions did not occur at the PAP site during our study, likely leading to the observed increase of bSiO_2 flux with depth. Nonsteady state conditions may lead to misinterpretation of particle attenuation rates both at PAP and at other sites where input fluxes from the upper ocean vary on the order of weeks, such as in polar and temperate regions with a strong seasonal cycle in export [Henson *et al.*, 2015].

3.4. Potential Error When Estimating Net Carbon Supply to the Mesopelagic Zone

Increases in bSiO_2 flux, and also iron or manganese fluxes, with depth have been observed previously in higher-latitude regions with pronounced seasonal blooms, such as at K2 (47°N , 160°E) during the VERTIGO project [Lamborg *et al.*, 2008]. These increases were attributed to lateral advection of suspended particulate matter. However, we here suggest that the increased flux with depth at these sites could have been, as was the case here, remnant material of the bloom, which had occurred 50–60 days before sampling took place

Low remineralization rates. Unfortunately, we have no direct measurements for the remineralization/dissolution rate of bSiO_2 at our study site. Yet we can estimate these rates indirectly. Rickert *et al.* [2002] measured dissolution kinetics of bSiO_2 collected from the surface, sediment traps, and sediments in different oceanic regimes, including material collected by sediment traps at 1000 m and 2500 m depth from the Norwegian Basin (70°N , 4°E). The data suggested that dissolution rates of bSiO_2 vary between the different regions, with natural samples dissolving fastest in the Norwegian Basin. Assuming that the bSiO_2 dissolution kinetics in the Norwegian Basin are similar to those at our study site, potential dissolution rates can be estimated using the reported equations for temperature-corrected solubility and dissolution rate coefficient (k) [Rickert *et al.*, 2002]. Temperatures at the PAP site were $\sim 15.5^\circ\text{C}$ at the surface and dropped to as low as 10°C at 600 m depth, with an average temperature of 11.6°C between 50 and 600 m. Solubility of

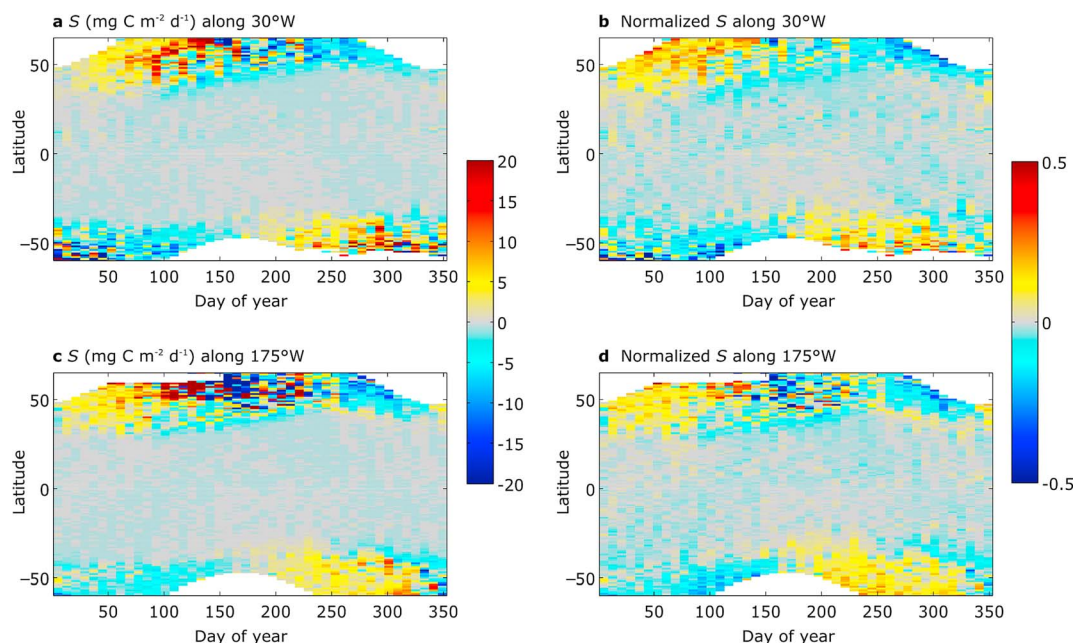


Figure 6. Seasonal variation in the potential error of estimated net POC supply to the upper mesopelagic zone (100–500 m depth) when assuming steady state (S). S ($\text{mg C m}^{-2} \text{d}^{-1}$) was calculated for two transects along the (a) Atlantic (30°W) and the (c) Pacific (175°W) using a satellite-derived climatology of export estimates, average sinking speeds of 40 m d^{-1} , and a temperature-corrected remineralization rate. S was then normalized to daily export ((b) Atlantic and (d) Pacific transects).

[Buesseler *et al.*, 2008]. We believe that our observation of nonsteady state conditions is an example of a more widespread phenomenon. This has significant implications for the interpretation of POC flux profiles and attempts to balance the net supply and demands of organic matter to the dark ocean.

We derived an equation that allows estimation of the magnitude of “misestimated” organic matter supply when assuming steady state (equation (6)). It is important to note that this “misestimate” can be either more or less organic matter supply than inferred when assuming steady state. For example, underestimates of net carbon supply increase when remineralization rates decrease (Table 1), sinking speeds slow down (column $a = 1.1 \text{ mg C m}^{-2} \text{d}^{-1}$), and/or the decrease in export flux accelerates (column $v = 50 \text{ m d}^{-1}$). Our equation can be easily applied to any situation where the time history of export flux prior to sampling is known.

For the PAP site in August 2009, the loss of POC was likely underestimated by $5\text{--}20 \text{ mg C m}^{-2} \text{d}^{-1}$ across the mesopelagic zone (mixed layer depth to 1000 m; Table 1). This is on the order of 5–22% of the net organic carbon supply at this site when assuming steady state ($92 \text{ mg C m}^{-2} \text{d}^{-1}$) [Giering *et al.*, 2014]. This analysis demonstrates quantitatively that ignoring temporal variability in flux could lead to some of the uncertainties surrounding imbalanced carbon budgets [Burd *et al.*, 2010].

We next illustrate on a global scale the potential range of error in estimated net POC supply to the upper mesopelagic zone (100–500 m depth) when assuming steady state (Figure 6). For this illustration, we assumed average sinking speeds of 40 m d^{-1} and a temperature-corrected remineralization rate (see section 2.2), though variations in these parameters will affect the predictions in a similar fashion as explored in Table 1 (Figure 7). We further used several combinations of algorithms for PP and e -ratio to see whether our estimates for S are robust. The median deviation away from the combination of algorithms used in the main text [Carr, 2001; Henson *et al.*, 2011] is $\sim 5\%$ and, although some combinations of algorithms show larger deviations, all show the same temporal evolution (Figure 8).

Largest errors in estimates of net POC supply to the mesopelagic zone are predicted for the high latitudes (50–65°N and 50–65°S) in both the Atlantic and Pacific (Figure 6). In our scenario (sinking speed of 40 m d^{-1} ; remineralization rate dependent on temperature), daily net POC supply is likely overestimated by up to $20 \text{ mg C m}^{-2} \text{d}^{-1}$ before the bloom, whereas it is likely underestimated by the same amount after the bloom (Figures 6a and 6c). As expected, estimates from regions with near constant export rates throughout the year (30°N to 30°S) are little affected when assuming steady state ($< 5 \text{ mg C m}^{-2} \text{d}^{-1}$; Figures 6a and 6c).

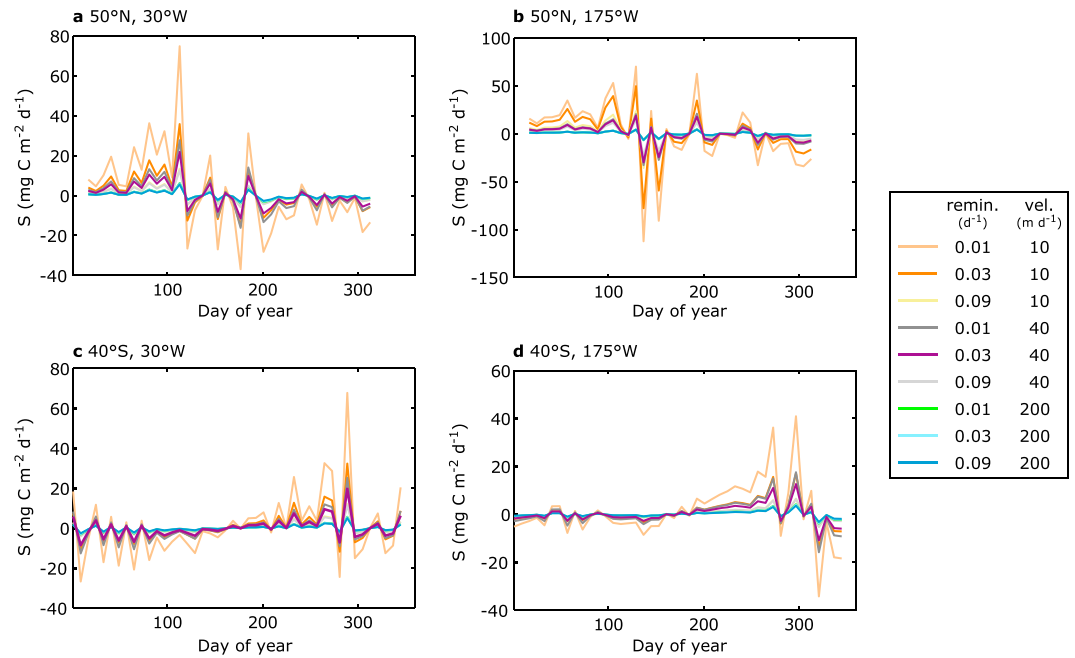


Figure 7. Sensitivity analysis of S (error in estimated net POC supply when assuming steady state) at four sites in the (a) North Atlantic (50°N, 30°W), (b) North Pacific (50°N, 175°W), (c) South Atlantic (40°S, 30°W), and (d) South Pacific (40°S, 175°W). S increases with decreasing remineralization rate (r in day⁻¹) and/or decreasing sinking speed (v in m d⁻¹). Combinations of v and r are presented as shown in legend.

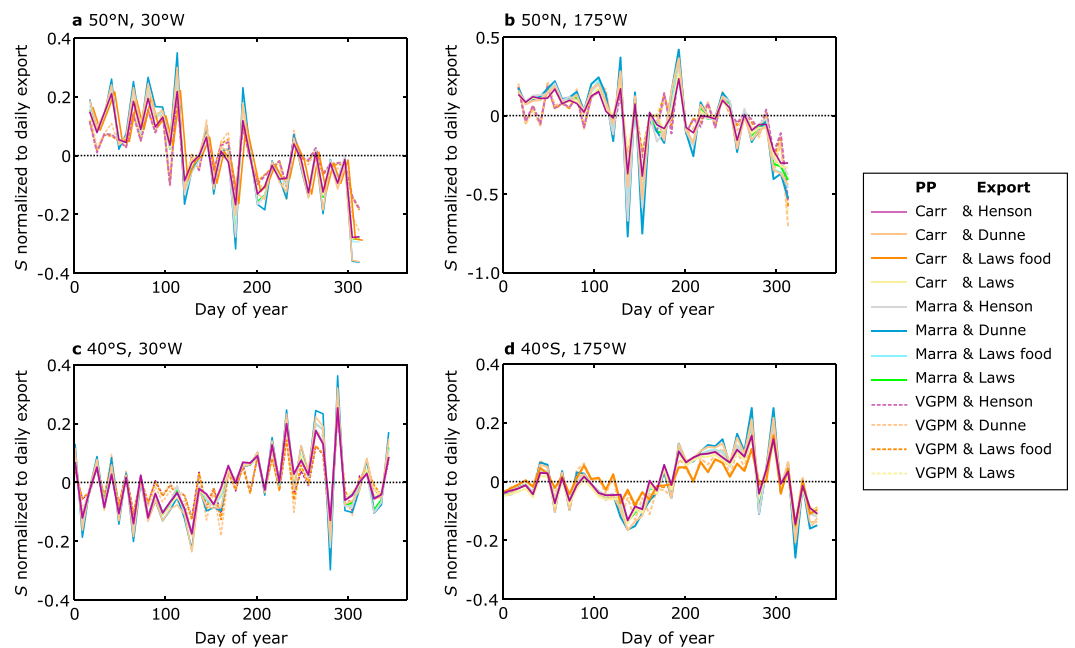


Figure 8. Time series of S normalized to daily export calculated using combinations of different algorithms for PP [Carr, 2001; Marra *et al.*, 2003; Behrenfeld and Falkowski, 1997] ("VGPM") and e -ratio [Dunne *et al.*, 2005; Henson *et al.*, 2011; Laws *et al.*, 2000] for four sites in the (a) North Atlantic (50°N, 30°W), (b) North Pacific (50°N, 175°W), (c) South Atlantic (40°S, 30°W), and (d) South Pacific (40°S, 175°W). Lines show permutations of the algorithms as shown in legend.

A similar global pattern emerges when normalizing S to daily export (Figures 6b and 6d). Errors in the tropics (30°N to 30°S) are low (<10%), and field campaigns in these regions (e.g., at ALOHA or Bermuda Atlantic Time Series) are likely unaffected when assuming steady state. Between 30 and 65°N and 30 and 65°S, two phases are prevalent: spring/summer before the peak of the bloom when net POC supply could be overestimated by $\leq 25\%$, and autumn after the peak of the bloom when net POC supply could be underestimated by $\leq 25\%$. Field campaigns in these regions (e.g., at PAP or K2) are thus likely to sample during nonsteady state conditions and are more susceptible to misinterpretation of particle flux profiles. For high-latitude regions (>65°N and >65°S) the estimates of POC loss in the model are poorly constrained. Nevertheless, potential errors are likely comparable to those of the temperate regions (30–65°)—if not higher—owing to the strong seasonality in these regions. Field campaigns investigating particle flux in high-latitude regions will have to pay careful attention when assuming steady state.

4. Conclusion

Sediment traps have been used extensively for determining particle flux and remineralization rates. The latter is calculated by comparing fluxes collected at different depths, which implies that the source (both composition and quantity) of the material caught in the traps is identical for these traps. However, our data suggest that this is likely not the case in temperate regions, where seasonal cycles cause large changes in export rates and composition throughout the year. As a large fraction of the sinking material may be sinking at slow rates (<40 m d⁻¹), these ecosystems do not operate at steady state, and the resulting interpretation of the flux profile is misleading. Net POC supply to the twilight zone may be wrong by as much as 25% when assuming steady state. Nevertheless, many flux campaigns take place in the post bloom period assuming that the system is at steady state. We here provide a simple equation to estimate the potential error when calculating carbon supply to the dark ocean during nonsteady state conditions. Future studies and methods (e.g., radio-tracer methods using ²³⁴Th and ²¹⁰Po) should consider this when interpreting flux profiles.

Acknowledgments

We thank the captain, crew, and scientist of the RRS Discovery during cruise D341; Kevin Saw and Sam Ward for deployment of PELAGRAS; and SAHFOS for CPR data (www.sahfos.ac.uk). Data from cruise D341 can be obtained from BODC (www.bodc.ac.uk). Model output and satellite products used in the paper can be obtained by emailing s.henson@noc.ac.uk. We thank four anonymous reviewers for their constructive criticism and the Natural Environmental Research Council (NERC) for support through National Capability funding.

References

- Alonso-González, I. J., J. Aristegui, J. C. Vilas, and A. Hernández-Guerra (2009), Lateral POC transport and consumption in surface and deep waters of the Canary Current region: A box model study, *Global Biogeochem. Cycles*, *23*, GB2007, doi:10.1029/2008GB003185.
- Alonso-González, I. J., J. Aristegui, C. Lee, A. Sanchez-Vidal, A. Calafat, J. Fabrés, P. Sangrá, P. Masqué, A. Hernández-Guerra, and V. Benítez-Barrios (2010), Role of slowly settling particles in the ocean carbon cycle, *Geophys. Res. Lett.*, *37*, L13608, doi:10.1029/2010GL043827.
- Behrenfeld, M. J., and P. G. Falkowski (1997), Photosynthetic rates derived from satellite-based chlorophyll concentration, *Limnol. Oceanogr.*, *42*(1), 1–20, doi:10.4319/lol.1997.42.1.0001.
- Berelson, W. M. (2002), Particle settling rates increase with depth in the ocean, *Deep Sea Res. Part II Top. Stud. Oceanogr.*, *49*(1–3), 237–251, doi:10.1016/S0967-0645(01)00102-3.
- Boyd, P. W., and T. W. Trull (2007), Understanding the export of biogenic particles in oceanic waters: Is there consensus?, *Prog. Oceanogr.*, *72*(4), 276–312, doi:10.1016/j.pocean.2006.10.007.
- Buesseler, K. O., et al. (2007), An assessment of the use of sediment traps for estimating upper ocean particle fluxes, *J. Mar. Res.*, *65*(3), 345–416.
- Buesseler, K. O., et al. (2008), VERTIGO (VERTical Transport In the Global Ocean): A study of particle sources and flux attenuation in the North Pacific, *Deep-Sea Res. II*, *55*(14–15), 1522–1539, doi:10.1016/j.dsr2.2008.04.024.
- Burd, A. B., and G. A. Jackson (2009), Particle aggregation, *Annu. Rev. Mar. Sci.*, *1*(1), 65–90, doi:10.1146/annurev.marine.010908.163904.
- Burd, A. B., et al. (2010), Assessing the apparent imbalance between geochemical and biochemical indicators of meso- and bathypelagic biological activity: What the @#! is wrong with present calculations of carbon budgets?, *Deep-Sea Res. II*, *57*(16), 1557–1571, doi:10.1016/j.dsr2.2010.02.022.
- Carr, M. E. (2001), Estimation of potential productivity in Eastern Boundary Currents using remote sensing, *Deep Sea Res. II*, *49*(1), 59–80, doi:10.1016/S0967-0645(01)00094-7.
- Conte, M. H., N. Ralph, and E. H. Ross (2001), Seasonal and interannual variability in deep ocean particle fluxes at the Oceanic Flux Program (OFP)/Bermuda Atlantic Time Series (BATS) site in the western Sargasso Sea near Bermuda, *Deep Sea Res. Part II Top. Stud. Oceanogr.*, *48*(8–9), 1471–1505, doi:10.1016/S0967-0645(00)00150-8.
- Doney, S. C., et al. (2004), Evaluating global ocean carbon models: The importance of realistic physics, *Global Biogeochem. Cycles*, *18*, GB3017, doi:10.1029/2003GB002150.
- Dunne, J. P., R. A. Armstrong, A. Gnanadesikan, and J. L. Sarmiento (2005), Empirical and mechanistic models for the particle export ratio, *Global Biogeochem. Cycles*, *19*, GB4026, doi:10.1029/2004GB002390.
- Gehlen, M., L. Bopp, N. Emprin, O. Aumont, C. Heinze, and O. Ragueneau (2006), Reconciling surface ocean productivity, export fluxes and sediment composition in a global biogeochemical ocean model, *Biogeosciences*, *3*(4), 521–537, doi:10.5194/bg-3-521-2006.
- Giering, S. L. C., et al. (2014), Reconciliation of the carbon budget in the ocean's twilight zone, *Nature*, *507*, 480–483, doi:10.1038/nature13123.
- Giering, S. L. C., R. Sanders, A. P. Martin, C. Lindemann, K. O. Möller, C. J. Daniels, D. J. Mayor, and M. A. S. John (2016), High export via small particles before the onset of the North Atlantic spring bloom, *J. Geophys. Res. Ocean.*, *121*, 6929–6945, doi:10.1002/2016JC012048.

- Henson, S. A., R. Sanders, E. Madsen, P. J. Morris, F. Le Moigne, and G. D. Quartly (2011), A reduced estimate of the strength of the ocean's biological carbon pump, *Geophys. Res. Lett.*, **38**, L04606, doi:10.1029/2011GL046735.
- Henson, S. A., R. Sanders, and E. Madsen (2012), Global patterns in efficiency of particulate organic carbon export and transfer to the deep ocean, *Global Biogeochem. Cycles*, **26**, GB1028, doi:10.1029/2011GB004099.
- Henson, S. A., S. C. Painter, N. P. Holliday, M. C. Stinchcombe, and S. L. C. Giering (2013), Unusual subpolar North Atlantic phytoplankton bloom in 2010: Volcanic fertilization or North Atlantic Oscillation?, *J. Geophys. Res. Oceans*, **118**, 4771–4780, doi:10.1002/jgrc.20363.
- Henson, S. A., A. Yool, and R. Sanders (2015), Variability in efficiency of particulate organic carbon export: A model study, *Global Biogeochem. Cycles*, **29**, 33–45, doi:10.1002/2014GB004965.
- Honjo, S., and S. J. Manganini (1992), Biogenic particle flux to the interior of the North Atlantic Ocean at the 34°N and 48°N stations, 1989/1990: Method and analytical data compilation, *WHOI Technical Report, WHOI-92-15*, 92(15), 1–74, doi:10.1594/PANGAEA.111885; doi:10.1594/PANGAEA.111886; doi:10.1594/PANGAEA.111887.
- Iversen, M. H., and H. Ploug (2010), Ballast minerals and the sinking carbon flux in the ocean: Carbon-specific respiration rates and sinking velocity of marine snow aggregates, *Biogeosciences*, **7**(9), 2613–2624, doi:10.5194/bg-7-2613-2010.
- Iversen, M. H., and H. Ploug (2013), Temperature effects on carbon-specific respiration rate and sinking velocity of diatom aggregates—potential implications for deep ocean export processes, *Biogeosciences*, **10**(6), 4073–4085, doi:10.5194/bg-10-4073-2013.
- Kwon, E. Y., F. Primeau, and J. L. Sarmiento (2009), The impact of remineralization depth on the air-sea carbon balance, *Nat. Geosci.*, **2**(9), 630–635, doi:10.1038/ngeo612.
- Lamborg, C. H., K. O. Buesseler, and P. J. Lam (2008), Sinking fluxes of minor and trace elements in the North Pacific Ocean measured during the VERTIGO program, *Deep Sea Res. II*, **55**(14), 1564–1577, doi:10.1016/j.dsr2.2008.04.012.
- Lampitt, R. S., B. J. Bett, K. Kiriakoulakis, E. E. Popova, O. Ragueneau, A. Vangriesheim, and G. A. Wolff (2001), Material supply to the abyssal seafloor in the Northeast Atlantic, *Prog. Oceanogr.*, **50**(1), 27–63, doi:10.1016/S0079-6611(01)00047-7.
- Lampitt, R. S., B. Boorman, L. Brown, M. Lucas, I. Salter, R. Sanders, K. Saw, S. Seeyave, S. J. Thomalla, and R. Turnewitsch (2008), Particle export from the euphotic zone: Estimates using a novel drifting sediment trap, ²³⁴Th and new production, *Deep-Sea Res. I*, **55**(11), 1484–1502, doi:10.1016/j.dsr.2008.07.002.
- Tomas, C. R. (Ed) (1997), *Identifying Marine Phytoplankton*, Academic Press, San Diego, Calif.
- Laws, E. A., P. G. Falkowski, W. O. Smith, H. Ducklow, and J. J. McCarthy (2000), Temperature effects on export production in the open ocean, *Global Biogeochem. Cycles*, **14**(4), 1231–1246, doi:10.1029/1999GB001229.
- Marra, J., C. Ho, and C. C. Trees (2003), An alternative algorithm for the calculation of primary production from remote sensing data, Rep. LDEO 2003–1, Lamont-Doherty Earth Obs., Palisades, New York.
- Martin, J. H., G. A. Knauer, D. M. Karl, and W. W. Broenkow (1987), VERTEX: Carbon cycling in the northeast Pacific, *Deep-Sea Res. A*, **34**(2), 267–285, doi:10.1016/0198-0149(87)90086-0.
- Martin, P., R. S. Lampitt, M. J. Perry, R. Sanders, C. Lee, and E. D'Asaro (2011), Export and mesopelagic particle flux during a North Atlantic spring diatom bloom, *Deep-Sea Res. I*, **58**, 338–349, doi:10.1016/J.DSR.2011.01.006.
- McDonnell, A. M. P., and K. O. Buesseler (2010), Variability in the average sinking velocity of marine particles, *Limnol. Oceanogr.*, **55**(5), 2085–2096, doi:10.4319/lo.2010.55.5.2085.
- Nelson, D. M., P. Tréguer, M. A. Brzezinski, A. Leynaert, and B. Quéguiner (1995), Production and dissolution of biogenic silica in the ocean: Revised global estimates, comparison with regional data and relationship to biogenic sedimentation, *Global Biogeochem. Cycles*, **9**(3), 359–372, doi:10.1029/95GB01070.
- Ragueneau, O., and P. Treguer (1994), Determination of biogenic silica in coastal waters: Applicability and limits of the alkaline digestion method, *Mar. Chem.*, **45**, 43–51, doi:10.1016/0304-4203(94)90090-6.
- Ragueneau, O., et al. (2000), A review of the Si cycle in the modern ocean: Recent progress and missing gaps in the application of biogenic opal as a paleoproductivity proxy, *Global Planet. Change*, **26**(4), 317–365, doi:10.1016/S0921-8181(00)00052-7.
- Richardson, A. J., A. W. Walne, A. W. G. John, T. D. Jonas, J. A. Lindley, D. W. Sims, D. Stevens, and M. Witt (2006), Using continuous plankton recorder data, *Prog. Oceanogr.*, **68**(1), 27–74, doi:10.1016/j.pocean.2005.09.011.
- Rickert, D., M. Schlüter, and K. Wallmann (2002), Dissolution kinetics of biogenic silica from the water column to the sediments, *Geochim. Cosmochim. Acta*, **66**(3), 439–455.
- Riley, J. S., R. Sanders, C. Marsay, F. A. C. Le Moigne, E. P. Achterberg, and A. J. Poulton (2012), The relative contribution of fast and slow sinking particles to ocean carbon export, *Global Biogeochem. Cycles*, **26**, GB1026, doi:10.1029/2011GB004085.
- Salter, I., R. S. Lampitt, R. Sanders, A. Poulton, A. E. S. Kemp, B. Boorman, K. Saw, and R. Pearce (2007), Estimating carbon, silica and diatom export from a naturally fertilised phytoplankton bloom in the Southern Ocean using PELAGRA: A novel drifting sediment trap, *Deep-Sea Res. II*, **54**, 2233–2259, doi:10.1016/J.DSR2.2007.06.008.
- Sanders, R. (2009), RRS Discovery Cruise D341, 8 Jul 2009– 13 Aug 2009, Oceans 2025 cruise report, National Oceanography Centre, Southampton, U. K.
- Sarmiento, J. L., and C. LeQuere (1996), Oceanic carbon dioxide uptake in a model of century-scale global warming, *Science*, **274**, 1346–1350, doi:10.1126/science.274.5291.1346.
- Siegel, D. A., E. Fields, and K. O. Buesseler (2008), A bottom-up view of the biological pump: Modeling source funnels above ocean sediment traps, *Deep Sea Res. Part I Oceanogr. Res. Pap.*, **55**(1), 108–127, doi:10.1016/j.dsr.2007.10.006.
- Torres Valdés, S., S. C. Painter, A. P. Martin, R. Sanders, and J. Felden (2014), Data compilation of fluxes of sedimenting material from sediment traps in the Atlantic Ocean, *Earth Syst. Sci. Data*, **6**, 123–145, doi:10.5194/essd-6-123-2014.
- Trull, T. W., S. G. Bray, K. O. Buesseler, C. H. Lamborg, S. Manganini, C. Moy, and J. Valdes (2008), In situ measurement of mesopelagic particle sinking rates and the control of carbon transfer to the ocean interior during the Vertical Flux in the Global Ocean (VERTIGO) voyages in the North Pacific, *Deep Sea Res., Part II*, **55**(14–15), 1684–1695, doi:10.1016/j.dsr2.2008.04.021.
- Turner, J. T. (2002), Zooplankton fecal pellets, marine snow and sinking phytoplankton blooms, *Aquat. Microb. Ecol.*, **27**, 57–102, doi:10.3354/ame027057.
- Villa-Alfageme, M., F. de Soto, F. A. C. Le Moigne, S. L. C. Giering, R. Sanders, and R. García-Tenorio (2014), Observations and modeling of slow-sinking particles in the twilight zone, *Global Biogeochem. Cycles*, **28**, 1327–1342, doi:10.1002/2014GB004981.
- Villa-Alfageme, M., F. C. de Soto, E. Ceballos, S. L. C. Giering, F. A. C. Le Moigne, S. Henson, J. L. Mas, and R. J. Sanders (2016), Geographical, seasonal, and depth variation in sinking particle speeds in the North Atlantic, *Geophys. Res. Lett.*, **43**, 8609–8616, doi:10.1002/2016GL069233.
- White, P. A., J. Kalf, J. B. Rasmussen, and J. M. Gasol (1991), The effect of temperature and algal biomass on bacterial production and specific growth rate in freshwater and marine habitats, *Microb. Ecol.*, **21**(1), 99–118, doi:10.1007/BF02539147.